Electronic Spectroscopy of Nonalternant Hydrocarbons Inside Helium Nanodroplets[†]

Özgür Birer,[‡] Paolo Moreschini,[‡] Kevin K. Lehmann,*[,§] and Giacinto Scoles[‡,‖,⊥]

Chemistry Department, Princeton University, Princeton, New Jersey 08544, Chemistry Department, University of Virginia, Charlottesville, Virginia 22903, Scoula Internazionale Superiore di Studi Avanzati, via Beirut 2-4, Trieste 34014, Italy, and Elettra, Sincrotrone Trieste S.C.p.A., Strada Statale 14 Km 163.5, Basovizza, Trieste 34012, Italy

We have recorded the electronic spectra of three polycyclic aromatic hydrocarbons (acenaphtylene, fluoranthene, and benzo(k)fluoranthene) containing a five-member ring and their van der Waals complexes with argon and oxygen with a molecular beam superfluid helium nanodroplet spectrometer. Although the molecules, which differ by addition of one or two fused benzene rings to acenaphtylene, have the same point group symmetry, the spectral lineshapes show distinct differences in the number of zero phonon lines and shapes of the phonon wings. Whereas the smallest molecule (acenaphtylene) has the most complicated line shape, the largest molecule (benzo(k)fluoranthene) shows different lineshapes for different vibronic transitions. The van der Waals complexes of fluoranthene exhibit more peaks than the theoretically allowed number of isomeric complexes with argon/oxygen. The current models of molecular solvation in liquid helium do not adequately explain these discrepancies.

1. Introduction

The electronic spectroscopy of quasi-one-dimensional fused polycyclic aromatic molecules (i.e., benzene,[1,2] naphthalene,[3] anthracene,[4] tetracene,[5−9] and pentacene[5,8,9]) inside helium nanodroplets has demonstrated the different solvation characteristics of these molecules. The vibronic spectra of these molecules consist of one or multiple sharp transitions (maximum full width at half maximum (fwhm) ~ 1 cm^{-1}), which are occasionally accompanied by a broad (~ 20 cm^{-1}) and weak ($\sim 10\%$ of the main peak under unsaturated conditions) peak at higher energy. The sharp transitions, which are the excitations of the chromophore inside the droplets, are called the zero phonon lines (ZPL). The broad structures, which are attributed to the simultaneous excitations of the compressional volume vibrations of the helium environment, are called the phonon wings (PWs). The first observation of the PW of glyoxal embedded in helium nanodroplets revealed that there is a ~ 5 cm^{-1} gap between the ZPL and the PW.[10] This gap has been attributed to the roton energy in the bulk superfluid helium in relation to the dispersion curve of elementary excitations and has been proposed as proof of superfluidity of the helium nanodroplets.[10] Benzene[1,2] and naphthalene[3] have single ZPLs without PWs. Anthracene[4] has several unresolved ZPLs and a broad PW starting immediately after the ZPLs. Tetracene[5−9] has two resolved ZPLs and a distinct PW with the characteristic roton gap and maxima.[10] Pentacene[5,8,9] has a single ZPL and a PW with an unusual fine structure. Because the interaction potential of helium with large polycyclic aromatic molecules is on the order of 80 cm^{-1}, one expects the localization of helium atoms in the first solvation shell.[6] This localization has been

thought to give rise to different structural isomers of the solvation shell and to cause splitting of the ZPLs.[6] The detailed experiments and calculations performed on tetracene inside helium nanodroplets suggested that both the ground and the excited states of tetracene are split into two levels.[6]

The separation of the potential minima above these types of molecules is typically 2.5 Å (distance between the centers of adjacent rings). This distance is smaller than the helium−helium distance in the bulk liquid (3.5 Å)[11] or the equilibrium distance of the helium dimer (2.96 Å with a D_e of 7.7 cm^{-1}).[12] At 2.5 Å, the He−He potential is repulsive with an energy of 15 cm^{-1}, which is twice the well depth.[12] Therefore, it was suggested that the helium atoms may not be able to simultaneously fill all of the minima.[6] The resulting combinations of the occupied sites give rise to isomers of the helium solvation shell and thus to the splitting of the spectrum of the chromophore molecule. There are a small number of isomers because the localization is more effective for the first solvation layer. Path integral Monte Carlo (PIMC) calculations of benzene in a He$_{39}$ cluster predicted that the He atoms above and below the plane of the molecule are completely localized.[13] Quantum Monte Carlo calculations of interaction of helium (up to 24 atoms) with planar polycyclic aromatic molecules also found strong localization of helium in the first solvent layer above and below the rings.[14] Similarly, PIMC calculations of phythalocyanine in a He$_N$ ($N_{max} = 150$) cluster indicate strong localization of the first solvation layer.[15] These calculations confirm that helium density in the first layer above the planar molecule is solid-like with a minimum separation of the peaks of 3.0 Å. Furthermore, it was proposed that splitting of the ZPL observed in emission[6b] in this case was due to transition from helium structures that are incommensurate to commensurate with the typography of the helium−molecule potential. In these Monte Carlo simulations, the potential interaction has been taken as the sum of the He−He dimer interactions and the pairwise addition of the He−X interactions, where X is an atom of the molecule.

* To whom correspondence should be addressed. E-mail: kl6c@virginia.edu; fax: (434) 243 2193.
‡ Princeton University.
§ University of Virginia.
‖ Scoula Internazionale Superiore di Studi Avanzati.
⊥ Sincrotrone Trieste S.C.p.A.

Nonalternant Hydrocarbons Inside Helium Nanodroplets

J. Phys. Chem. A, Vol. 111, No. 49, 2007 **12201**

Although the three body forces were excluded, the calculated spectral shifts were comparable to the experimental results.[15] Therefore, the interaction of a single helium atom with a large polycyclic molecule is regarded as descriptive of the environment of a molecule inside helium droplets. All the calculations on doped helium droplets, we are aware of, have used the pairwise addition approximation.[6,8,13−15] The appearance of the splitting pattern was reported to sensitively depend on the first solvation layer. Addition of an Ar atom to the tetracene molecule quenched the splitting completely.[5] However, we have demonstrated in our laboratory that biphenylene, with a separation of 3.85 Å between the minima positions, still has split ZPLs, although these positions can be occupied at the same time without yielding any structural isomers of the solvation shell.[16] Furthermore, the splitting was retained upon complexation with an argon atom, unlike the tetracene case. Therefore, at this point, our understanding of helium solvation of these molecules and its relationship to the observed lineshapes is incomplete (i.e., even a qualitative prediction of the line shape observed in a new molecule based on the previous experiments is still not possible).

In this study, we present the helium nanodroplet isolation (HENDI) electronic spectroscopy of a new class of polycyclic aromatic hydrocarbons containing a five-member ring to broaden our experience and understanding of helium solvation. We have studied the $S_1 \leftarrow S_0$ electronic transition of acenaphtylene, fluoranthene, and benzo(k)fluoranthene and their van der Waals complexes inside helium nanodroplets using the beam depletion method. Acenaphtylene, fluoranthene, and benzo(k)fluoranthene constitute a series of nonalternant aromatic molecules that differ by sequential addition of a fused benzene ring. Unlike the polyacenes with delocalized electron density, these nonalternant hydrocarbons with $4n$ π electrons can exhibit distinct single and double C−C bond characteristics due to more localized electron density.

The first impression of these molecules is that they are composed of two-component subsystems: naphthalene−ethylene for acenaphtylene, naphthalene−benzene for fluoranthene, and naphthalene−naphthalene for benzo(k)fluoranthene. However, in a series of papers, Michl et al. demonstrated that lower excited states of acenaphtylene and fluoranthene do not correlate to the excited states of benzene or naphthalene.[17]

Although acenaphtylene, fluoranthene, and benzo(k)fluoranthene are similar compounds, they exhibit different photophysical properties following $S_1 \leftarrow S_0$ transitions. Acenaphtylene has low oscillator strength ($f_{exp} \sim 0.005$), and it is nonfluorescent. Fluoranthene also has low oscillator strength ($f_{exp} \sim 0.012$), but it has a moderate quantum fluorescence yield (~ 0.3). Benzo-(k)fluoranthene has high oscillator strength, and it has a near unity fluorescence quantum. Low-temperature matrix isolation spectra of all three compounds exist,[18] but only for fluoranthene is there a published jet-cooled single vibronic level resolved spectrum.[19] High-resolution spectra of acenaphtylene and benzo-(k)fluoranthene are reported in this study for the first time. We point out that the combination of five- and six-membered rings is the structural motif on which many important materials are based, such as the fullerenes and the termination of single wall carbon nanotubes (SWCNTs). Because SWCNTs are being used or considered for countless applications in nanoelectronics and scanning probe stimulated spectroscopy, the present study may provide information useful in these fields.

2. Experimental Section

The experiments were carried out on the Princeton droplet spectrometer, which was previously described in detail.[20] The
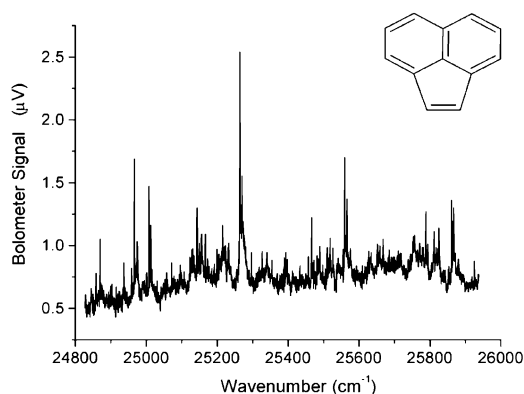

Figure 1. The $S_1 \leftarrow S_0$ electronic transition of acenaphtylene inside helium droplets.

spectrometer has two differentially pumped chambers, each evacuated by oil diffusion pumps. A 10 μm nozzle in the source chamber is cooled to 17 K by closed cycle refrigerators. Ultrapure (99.9999%) helium gas at 50 bar pressure is expanded into vacuum to form droplets with a mean size of 6500 atoms/droplet.[21] A 390 μm diameter skimmer is located about 1 cm from the nozzle, leading into the detection chamber. In that chamber, there are two ovens and one gas scattering box used as pickup cells to load the droplets with the dopant(s) under study. The organic molecules (>99%, Aldrich) are heated in the ovens to a vapor pressure of about 10^{-4} Torr. The gas pickup cell is used to create the van der Waals complexes of the organics with argon or oxygen. The doped droplets interact with the laser in a multipass cell, which is composed of two flat, high reflector mirrors. The detector is an optothermal bolometer,[22] which monitors the flux of the droplet beam. The bolometer has a specified noise equivalent power of 0.13 pW/$\sqrt{\text{Hz}}$, which translates to about 100 nV of noise under experimental conditions. The droplet beam signal is $\sim$13 mV, and is detected with a chopping frequency of 21 Hz. When an electronically excited molecule relaxes radiatively (nonradiatively) from the excited state, it deposits a fraction (all) of its excitation energy to the droplet, causing evaporation and shrinkage in size. (In the radiative case, the droplet deposited energy arises from the Stokes shift on emission). The bolometer detects the depletion in beam flux when the laser is on resonance with an electronic transition. The bolometer signal was amplified first by a cold J230 JFET,[22] then by a Stanford SR550 preamplifier, and finally demodulated by a Stanford SR510 lock-in amplifier. Although this setup is ideal for non- or weakly-fluorescent species (i.e., acenaphtylene), we could also record the spectra of fluorescent molecules (i.e., fluoranthene and benzo(k)fluoranthene) with optimized conditions.

The optical radiation source was a frequency doubled Ti:Al₂O₃ laser, which is a modified Indigo[23] system running with the Littman cavity[24] design. The Indigo was pumped by an Evolution-30,[23] a diode pumped, intracavity frequency doubled Nd:YLF laser. The second harmonic of the Ti:Al₂O₃ laser was generated by an angle tuned LBO crystal. The laser can scan about 2000 cm⁻¹ in the second harmonic region with a line width less than 0.2 cm⁻¹. The average pulse energy was about 150 μJ, and the pulse width was $\sim$10 ns. The laser fundamental wavelength was monitored by a Burleigh WA-4500 wavemeter.[25] The frequency calibration was achieved with a 7 cm⁻¹ free spectral range Etalon and a Ni−Ne hollow cathode optogalvanic lamp. Because of the limited frequency response of the bolometer, the 1 kHz repetition rate of the laser was reduced to 250 Hz by modulation with a reflective chopper. The reflected pulses from the chopper wheel were used to

TABLE 1: Calculated and Experimental S_n Term Values and Oscillator Strengths (f) of Acenaphtylene

	$S_1 - {}^1B_2$ (cm^{-1})	f	$S_2 - {}^1A_1$ (cm^{-1})	f	$S_3 - {}^1B_2$ (cm^{-1})	f
experimental[a]	21 390	0.005	29 310	0.1	30 950	0.2
SCI[b]	22 110	0.003	29 980	0.07	30 320	0.06
SECI−1[c]	23 990	0.03	29 890	0.15	30 350	0.10
TD−DFT/SVWN[d]	22 745	0.004	29 036	0.075	31 698	0.078
TD−DFT/BLYP[d]	22 664	0.005	28 875	0.077	31 456	0.078
TD−DFT/B3LYP[d]	24 842	0.006	31 053	0.105	33 553	0.098
experimental[e]	21 454	0.004	29 520	0.165	31 053	
TD−DFT/B3LYP[f]	24 858	0.006	31 022	0.096	33 540	0.091

a From ref 29, spectrum recorded in a 3-methylpentane matrix at 77 K. *b* From ref 29, all singly excited configurations. *c* From ref 29, selected singly and doubly excited configurations. *d* From ref 31. *e* From ref 31, spectrum recorded in Argon matrix at 12 K. *f* This work.

monitor the laser power. The control of the laser system and data acquisition were performed with a PC running a custom program written in Labview.[26]

Normal modes were calculated at the density functional theory (DFT) using the B3LYP functional and restricted Hartree−Fock (RHF) levels in the ground electronic state and the latter's (almost) equivalent RCIS level in the first excited state,[27] using the 6-311+G(d,p) basis set. The energy and oscillator strength of the low lying electronic transitions were calculated at the time dependent DFT (TD−DFT), also using the B3LYP functional. The Gaussian03 package was used for these calculations.[28]
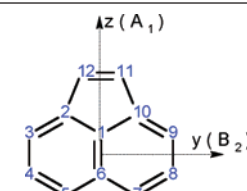
3. Results

3.1. Electronic Spectroscopy of Acenaphtylene In Helium Nanodroplets.

Acenaphtylene (see Figure 1 for structure) is a planar molecule with 12 π electrons. It has extremely low quantum fluorescence yield ($\sim 10^{-4}$), which makes it suitable for a HENDI depletion experiment. The electronic states of acenaphtylene have been studied both experimentally and theoretically.[29−31]

The $S_1 \leftarrow S_0$ transition is weak but is symmetry allowed with a low molar extinction coefficient ($\epsilon \sim 100$ M^{-1} cm^{-1}) and is polarized along the long axis of the molecule.[29] Previous calculations, summarized in Table 1, have been performed using semiempirical π-electron self-consistent field configuration interaction (SCF−CI) Pariser−Parr−Pople[29] and, recently, using TD−DFT.[31] All previous spectroscopy has been in some form of matrix; thus, the reported experimental transition wavenumbers are expected to be red-shifted by a couple hundred cm^{-1} from those of an isolated molecule. On the basis of prior data, we estimated the electronic origin of the isolated molecule to be around 22 000 cm^{-1}.

We have calculated the bond lengths in the ground and first excited states to deduce the geometry change upon electronic excitation. Our ground state calculations agree with previous reported calculations and the experiment.[32,33] The results are summarized in Table 2. The presence of distinct single and double C−C bonds in the ground electronic state demonstrates the molecule's localized electron distribution. Upon electronic excitation, naphthalene and ethylene moieties approach each other because the symmetric arms of the five-member ring shorten. An elongation of the ethylene double bond is also predicted. The large geometrical change is thought to disturb the helium solvation shell around the molecule and to give rise to a strong and broad PW.

The $S_1 \leftarrow S_0$ electronic transition of acenaphtylene inside helium nanodroplets is presented in Figure 1. Unfortunately, only a couple of vibronic transitions are in the spectral region accessible to us. If we use our estimation for the electronic origin (22 000 cm^{-1}), then the vibronic transitions in the HENDI spectrum should include modes of C−H stretches and overtones and combinations of lower frequency modes. However, it is difficult to assign the lines with the current amount of information, especially without the exact position of the 0_0^0 transition.

The expanded view of the strongest acenaphtylene vibronic transition is presented in Figure 2. The peak is composed of four sharp (fwhm ~ 1 cm^{-1}) peaks riding on a broad background, which is interpreted as the PW. The peak shape is similar to the peak shape of perylene for $S_1 \leftarrow S_0$ transition inside helium droplets recorded under high resolution. However, the similarity is only qualitative, because the pattern in this case is on a larger scale. For perylene, the lines are as narrow as 0.25 cm^{-1}, and the PW extends about 15 cm^{-1} to the blue. In the acenaphtylene case, the sharpest line is about 0.75 cm^{-1} wide, and the PW extends to about 30 cm^{-1}. It is noted that the spectra in ref 9 were recorded using a narrow line width continuous wave (CW) laser and laser-induced fluorescence (LIF) detection. The spectrum presented here was recorded with a pulsed laser and depletion detection. Despite the use of a pulsed laser source, the spectra were unsaturated.

3.2. Fluoranthene.

3.2.1. Electronic Spectroscopy of Fluoranthene In Helium Nanodroplets. Fluoranthene is a nonalternant hydrocarbon with 16 π electrons. The molecule is composed of two aromatic moieties: benzene and naphthalene fractions joined by a five-member ring. Although the molecule is larger than acenaphtylene by a benzene ring, its $S_1 \leftarrow S_0$ transition lies higher in energy as compared to that of acenaphtylene. The transition is symmetry allowed, but it carries low oscillator strength. The observed moderate intensity transition ($\epsilon \sim 10^3$ M^{-1} cm^{-1}) is due to vibronic coupling to higher excited states.[34] Fluoranthene has a fluorescence quantum yield of 0.3 and a fluorescence lifetime of 58 ns (in rigid glass at 77 K).[35] This molecule has been studied experimentally and theoretically by several groups.[19,36−39] Electronic states have been determined by low-temperature matrix isolation and magnetic circular dichroism spectroscopy and SCF−CI PPP calculations.[36] Dantus and Chan recorded the $S_1 \leftarrow S_0$ transition with single vibronic level resolution for jet-cooled samples.[19] Infrared (IR) spectra
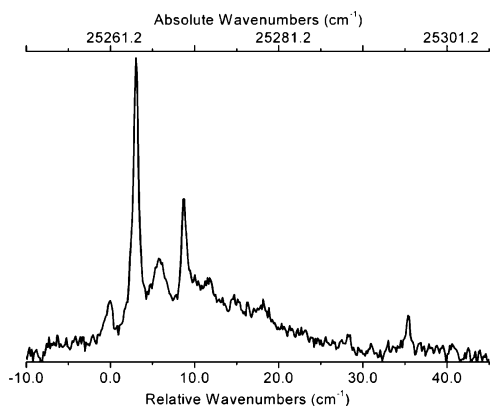
TABLE 2: Calculated and Experimental Bond Lengths (Å) of Acenaphtylene

	bond	exp[a]	BPW91[b]	B3LYP[c]	RHF[d]	CIS[e] (S_1)
	C1−C2	1.441	1.420	1.415	1.409	1.437
	C2−C3	1.381	1.388	1.379	1.360	1.410
	C3−C4	1.424	1.427	1.424	1.427	1.383
	C4−C5	1.382	1.391	1.383	1.366	1.405
	C5−C6	1.433	1.429	1.425	1.425	1.406
	C1−C6	1.386	1.402	1.394	1.377	1.407
	C2−C12	1.466	1.472	1.473	1.480	1.389
	C11−C12	1.395	1.372	1.362	1.341	1.441

a From ref 33, neutron diffraction at 80 K. *b* From ref 32. *c−e* This work.

Nonalternant Hydrocarbons Inside Helium Nanodroplets

J. Phys. Chem. A, Vol. 111, No. 49, 2007 **12203**

Figure 2. Typical single vibronic level line shape for $S_1 - S_0$ transition of acenaphtylene in helium droplets.

of fluoranthene in a low-temperature *n*-pentane matrix[40] and at room temperature[38] (as KBr and polyethylene pellets and as Nujol mulls) have been reported and compared to force field calculations.[38]

The experimental and calculated energies of the first three singlet excited states together with their oscillator strengths are presented in Table 3. The experimental values are taken from Shi'polskii matrix spectra that are red-shifted from the actual values. The weak $S_1 \leftarrow S_0$ transition cannot be observed at room temperature, and it is only a shoulder of the stronger $S_2 \leftarrow S_0$ transition at 77 K. The jet spectrum of Chan and Dantus places the electronic origin of the $S_1 \leftarrow S_0$ transition at 25 210 cm^{-1}. Calculations using TD$-$DFT perform no better than the semiempirical PPP calculations, and they both overestimate the S_1 term value by about 1800 cm^{-1}. Although the experimental $S_1 - S_2$ gap is around 3000 cm^{-1}, theoretical calculations predict a gap of about half as much. The configuration interaction singles (CIS) method overestimated the $S_1 - S_2$ spacing by about 10 000 cm^{-1}. The relatively small $S_1 - S_2$ gap couples these states, and fluoranthene is known to exhibit fluorescence from the S_2 to the S_0 state in condensed phase,[35] which is an exception to Kasha's rule.

The bond lengths of fluoranthene have been calculated for the ground state and for the first singlet excited state using different levels of theory (see Table 4). The ground state calculations performed with PPP, B3LYP, and RHF levels agree with the experimental values obtained by X-ray diffraction.[41] Overall, DFT with B3LYP functional estimates the bond lengths more accurately than the other two methods. The naphthalene part of the molecule exhibits the expected bond alternation, but the benzene moiety has almost uniform bond lengths except for the bond that is part of the five-member ring. Following the electronic excitation, much like in acenaphtylene, the symmetric arms of the five-member ring shrink, bringing the benzene and naphthalene moieties closer. Consequently, the benzene ring expands along the short axis of the molecule.

We have recorded the $S_1 \leftarrow S_0$ spectrum of fluoranthene and its van der Waals complexes with argon and oxygen inside helium droplets using depletion detection. The HENDI spectrum is similar to the reported jet spectrum with a better signal-to-noise ratio, especially for the higher vibronic bands as presented in Figure 3. The HENDI spectrum has about 100 peaks spanning more than 2000 cm^{-1}.

A comparison of the positions of four major lines (explicitly labeled a$-$d in ref 19) in the HENDI and jet spectra is presented in Table 5. The red-shift inside the droplets is relatively large and is not the same for all modes. The smallest shift is for purely electronic 0_0^0 transition, which has almost half the shift of the

higher vibronic transitions. This is an unusual difference; for perylene, the observed droplet shift for the vibronic bands is 1$-$6 cm^{-1} less than the shift of the electronic origin.[42] For benzene,[1] pentacene,[5,6] and tetracene,[5,6] the droplet induced shifts for the vibronic transitions are within 10 cm^{-1} of the shift of the electronic origin. In IR spectra in droplets, vibrational wavenumber shifts of only a few cm^{-1} are typical.[20]

Because the oscillator strength of fluoranthene is very small, the observed strong peaks in the spectrum steal intensity by Herzberg$-$Teller coupling from the higher excited states. Although Chan and Dantus established that the coupling modes should have b_2 symmetry, because of their poor signal-to-noise in the higher frequency part of the spectrum, they could only identify one such mode. Although it is not possible to make definite peak assignments without emission spectra, the peaks marked with an asterisk in Figure 3 are tentatively assigned to b_2 normal modes using the calculated frequencies in the ground and excited states, which are listed in Table 6. The unscaled RHF and CIS results are used for the purpose of showing the expected change in the frequency of the mode. B3LYP results are scaled by a factor of 0.9656 to match the experimental Raman spectrum.

The lineshapes for all the fluoranthene vibronic bands are similar. A typical peak is expanded in Figure 4. A narrow ZPL (fwhm $\sim$ 0.40 cm^{-1}) is followed by a weak peak about 2.3 cm^{-1} on the high-energy side. The weak PW following the ZPL extends about 20 cm^{-1} with a maximum at 6.4 cm^{-1} relative to the ZPL. This maxima of the phonon wing coincides with the estimate for roton excitations in the droplet.[10]

3.2.2. Fluoranthene van der Waals Complexes with Argon and Oxygen. The $S_1 \leftarrow S_0$ transition of van der Waals complexes of fluoranthene with argon and oxygen inside helium droplets near the electronic origin are shown in Figures 5 and 6, respectively. In both cases, four peaks can be partially resolved that are red-shifted about 40 cm^{-1}. The gas pick-up pressure dependence of these peaks is the same, which means they are all 1:1 complexes. Please note that there are only three inequivalent helium ring binding sites on top of the fluoranthene molecule, and thus there is not a simple association between the number of ZPLs and the number of inequivalent local deep minima in the He$-$molecule potential energy function.

3.3. Benzo(k)fluoranthene. *3.3.1. Electronic Spectroscopy of Benzo(k)fluoranthene In Helium Nanodroplets.* Benzo(k)-fluoranthene has been studied by Michl with low-resolution UV$-$vis spectroscopies.[43,44] The glass matrix spectrum was recorded and PPP calculations were compared to experimental results. The $S_1 \leftarrow S_0$ transition is allowed and is strong ($\epsilon \sim$ 10^4 M^{-1} cm^{-1}). It has almost unity quantum yield for fluorescence in solution with a lifetime of 7.8 ns.[45] The S_1 transition is polarized in the long axis direction, contrary to acenaphtylene and fluoranthene, which are polarized along the long axis of the naphthalene moiety. The high-resolution spectrum of this molecule has not been reported until now.

The experimental and calculated term values of the first three singlet excited states together with oscillator strengths are presented in Table 7. The experimental value is taken from solution-phase spectra, which are red-shifted from the isolated molecule value. Transitions to the second and third singlet excited states carry extremely low oscillator strengths, and they are not observed by low-resolution methods. The S_1 of this molecule has the same electronic character as that of the S_2 state in the above-discussed molecules.

There are no reports on the experimental or calculated bond lengths of this molecule. Table 8 summarizes our calculations

TABLE 3: Term Values and Oscillator Strengths (f) of Fluoranthene $S_n \leftarrow S_0$ Transitions

	experimental[a]		PPP[b]		CIS[c]		TD-DFT[c]	
state	T_n (cm^{-1})	f	T_n (cm^{-1})	f	T_n (cm^{-1})	f	T_n (cm^{-1})	f
$S_1-{}^1B_2$	24 750	0.012	27 000	0.014	36 623	0.0092	26 996	0.0041
$S_2-{}^1A_1$	27 750	0.17	28 000	0.52	38 171	0.3781	28 689	0.1654
$S_3-{}^1B_2$	30 950	0.05	32 000	0.08	42 479	0.0589	33 333	0.0266

[a] From ref 36, spectra taken in a 3-Methylpentane matrix at 77 K. [b] From ref 36, SCF−CI PPP calculation. [c] This work.

TABLE 4: Calculated and Experimental Bond Lengths (Å) of Fluoranthene

bond	exp.[a]	PPP[b]	B3LYP[c]	RHF[c]	PPP[d] (S_1)	CIS[c] (S_1)
C1−C2	1.414	1.428	1.416	1.412	1.444	1.436
C2−C3	1.374	1.390	1.378	1.360	1.414	1.403
C3−C4	1.415	1.416	1.422	1.425	1.405	1.390
C4−C5	1.372	1.384	1.383	1.366	1.400	1.399
C5−C6	1.426	1.425	1.423	1.423	1.425	1.411
C1−C6	1.404	1.415	1.400	1.382	1.415	1.406
C2−C12	1.480	1.464	1.476	1.482	1.431	1.407
C11−C12	1.415	1.410	1.425	1.409	1.451	1.481
C12−C13	1.392	1.404	1.390	1.380	1.418	1.415
C13−C14	1.388	1.398	1.398	1.391	1.389	1.361
C14−C15	1.384	1.402	1.396	1.386	1.427	1.440

[a] From ref 41, X-ray diffraction results. [b] From ref 36, SCF−CI PPP approximation for the S_0 state. [c] This work. [d] From ref 36, SCF−CI PPP approximation for the S_1 state.

TABLE 5: Comparison of Selected Peak Positions for Jet and HENDI $S_1 \leftarrow S_0$ Spectra of Fluoranthene

jet[19]		HENDI		
absolute (cm^{-1})	relative (cm^{-1})	absolute (cm^{-1})	relative (cm^{-1})	shift (cm^{-1})
25 209.8	0.0	25 185.7	0.0	−24.1
25 637.1	427.3	25 595.8	410.1	−41.3
25 960.6	750.8	25 915.4	729.7	−45.2
26 554.4	1344.6	26 514.1	1328.7	−40.3

TABLE 6: Absolute and Relative Wavenumbers of Possible Fluoranthene Transitions with b_2 Symmetry

position[a] (cm^{-1})	excess[b] (cm^{-1})	B3LYP[c] (S_0) (cm^{-1})	RHF[d] (S_0) (cm^{-1})	CIS[d] (S_1) (cm^{-1})
25 381.2	195.4	203	222	219
25 595.8	410.1	471	508	433
25 943.2	757.5	766	826	797
26 243.3	1057.6	1090	1172	1153
26 312.3	1126.6	1150	1209	1173
26 374.8	1189.1	1236	1344	1335
26 514.2	1328.5	1375	1470	1443
26 647.0	1461.6	1478	1623	1583

[a] Experimental values from the HENDI spectrum. [b] Calculated with respect to the electronic origin at 25 185.7 cm^{-1}. [c] Scaled to the experimental Raman spectrum. [d] Unscaled.
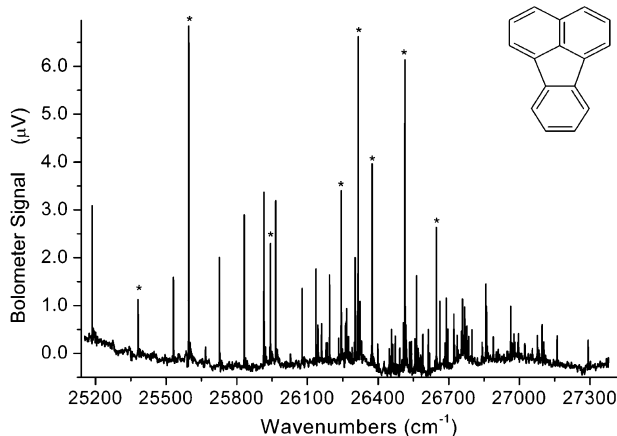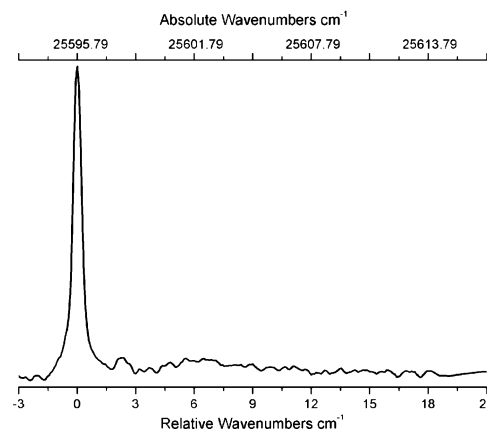

Figure 3. $S_1 \leftarrow S_0$ spectrum of fluoranthene inside helium nanodroplets. The * indicates modes with b_2 symmetry (see text for details).

Figure 4. Expanded view of a typical line shape for the fluoranthene $S_1 \leftarrow S_0$ transition.

at TD−DFT/B3LYP and RHF levels for the ground and CIS level for the first excited electronic states. Contrary to acenaphtylene and fluoranthene, the shortening of the symmetric bonds of the five-member ring is not significant.

The $S_1 \leftarrow S_0$ spectrum of benzo(k)fluoranthene in helium nanodroplets is presented in Figure 7. The spectrum spans ~2000 cm^{-1} above the 0_0^0 transition. Single vibronic lines are resolved up to ~1000 cm^{-1} excess energy. Around 27 000 cm^{-1}, a broad structure with multiple sharp lines emerges.

This broad structure cannot be attributed to the $S_2 \leftarrow S_0$ transition because theoretically it carries extremely small oscillator strength. In addition, the calculated S_1-S_2 gap of 2250 cm^{-1} is probably a severe underestimation, because the calculated S_1-S_2 gap for fluoranthene, with the same level of

theory and basis set, is almost half the experimental value. Because the ground and excited states have A_1 symmetry, the observed spectrum can be explained by the allowed vibronic transitions of a_1 symmetry. Table 9 presents the list of the strongest peaks and ground state energies of the possible a_1 modes (in-plane bending and ring-breathing) corresponding to that transition. The calculated frequencies are scaled by a factor of 0.9427 to match the experimental Raman spectrum. Around 27 000 cm^{-1}, or about 1400 cm^{-1} excess energy above the

Nonalternant Hydrocarbons Inside Helium Nanodroplets

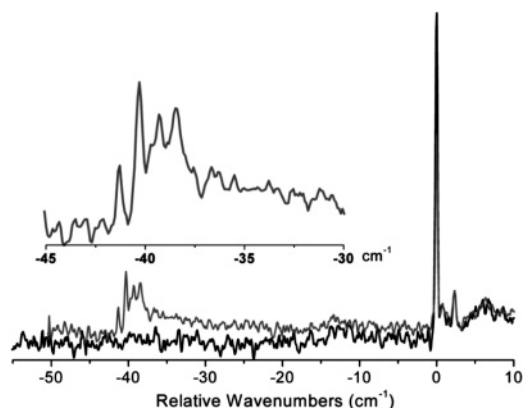*J. Phys. Chem. A, Vol. 111, No. 49, 2007* **12205**

Figure 5. Spectrum of the fluoranthene−argon complex inside helium nanodroplets near the electronic origin.
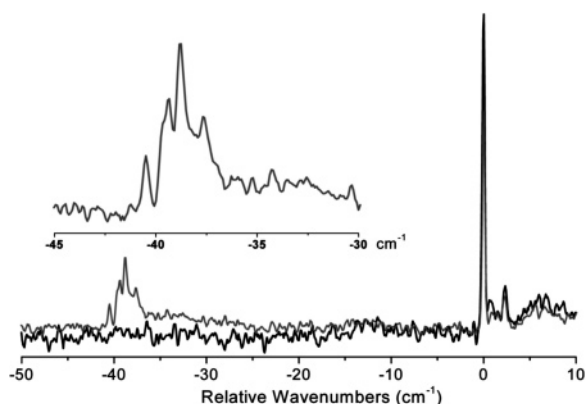

Figure 6. Spectrum of the fluoranthene−oxygen complex inside helium nanodroplets near the electronic origin.

TABLE 7: Term Values and Oscillator Strengths of $S_n \leftarrow S_0$ Transitions of Benzo(k)fluoranthene

state	experimental[a]		PPP[b]		TD−DFT/B3LYP[c]	
	T_n (cm^{-1})	f	T_n (cm^{-1})	f	T_n (cm^{-1})	f
$S_1-{}^1A_1$	24 900	0.21	25 700	0.23	25 891	0.22
$S_2-{}^1B_2$			28 300	0.000 09	28 131	0.0007
$S_3-{}^1B_2$			30 700	0.000 41	29 899	0.0069

[a] From ref 43 spectra taken at room temperature in cyclohexane. [b] From ref 43 SCF−CI PPP calculation. [c] This work.

TABLE 8: Calculated Bond Lengths (Å) of Benzo(k)fluoranthene in S_0 and S_1 States

bond	B3LYP (S_0)	RHF (S_0)	CIS (S_1)
C1−C2	1.412	1.412	1.423
C2−C3	1.379	1.360	1.384
C3−C4	1.421	1.423	1.426
C4−C5	1.383	1.366	1.389
C5−C6	1.423	1.422	1.427
C1−C6	1.403	1.385	1.407
C2−C12	1.474	1.481	1.478
C11−C12	1.447	1.440	1.455
C12−C13	1.370	1.353	1.374
C13−C14	1.424	1.425	1.429
C14−C15	1.435	1.411	1.441
C15−C17	1.418	1.417	1.422
C17−C18	1.376	1.361	1.383
C18−C19	1.413	1.413	1.417
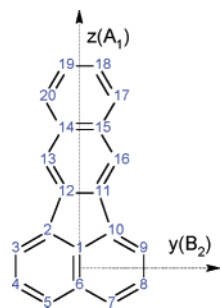
electronic origin, there are eight closely spaced a_1 modes, which are responsible for the observed structure. These are the highest a_1 normal mode fundamentals before the C−H stretching region. Following this group, there are only three b_2 modes before the C−H stretching region, which are responsible for the weak absorptions in the last part of the spectrum.
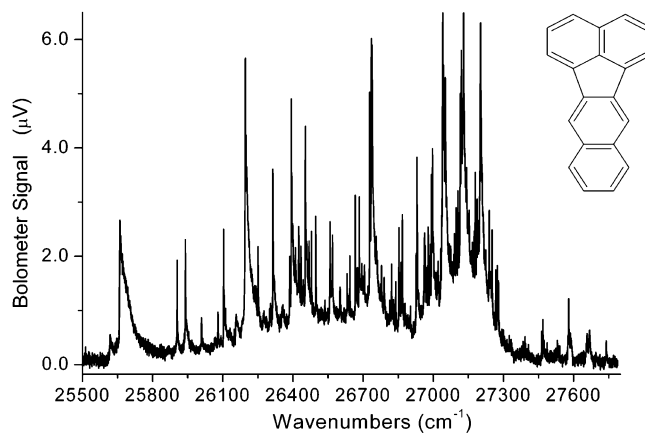

Figure 7. $S_1 \leftarrow S_0$ transition of benzo(k)fluoranthene in helium nanodroplets.

TABLE 9: Positions of Strongest Benzo(k)fluoranthene Vibronic Peaks and Calculated (scaled) a_1 Normal Modes

position (cm^{-1})	excess energy (cm^{-1})	scaled S_0 frequency (cm^{-1})
25 657.8	0.0	
25 940.1	282.3	277.5
26 103.3	445.5	441.2
26 196.4	538.6	541.2
26 313.8	656.0	652.9
26 392.9	735.1	736.0
26 453.1	795.3	782.8
26 735.2	1077.4	1056.3
26 930.4	1272.6	1240.0
26 996.8	1339.0	1330.2
27 040.8	1383.0	1380.4
27 129.7	1471.9	1469.5
27 201.8	1544.0	1537.7

Contrary to all other molecules studied inside helium nanodroplets, there are several different types of peak shapes in the spectral window. The electronic origin located at 25 658 cm^{-1} has a broader peak shape compared to the rest of the spectra. Until the broad structure around 27 000 cm^{-1}, the intense peaks have split ZPL with an approximately 3:2 intensity ratio followed by a PW. On the other hand, for some of the weak lines the splitting is not resolved. The lineshapes for vibronic bands above 27 000 cm^{-1} are much broader, and a ZPL splitting is not observed.

The expanded view of the 0_0^0 transition of benzo(k)fluoranthene is presented in Figure 8. The peak is composed of two partially resolved narrow ZPLs separated by 2.3 cm^{-1}. The ZPL with higher energy is more intense than the other. An intense and broad PW extends about 150 cm^{-1} to the blue side. The PW has a distinct maxima at 6.1 cm^{-1}, which agrees with the location of roton excitations. However, unlike other spectra, there is no gap between the ZPL and the roton maxima of the PW.

An expanded view of the vibronic transition around 26 400 cm^{-1} is presented in Figure 9. This intense band has two ZPLs separated by 2.6 cm^{-1} and a maxima at 6.0 cm^{-1} is observed on the PW. Contrary to the 0_0^0 transition, the ZPL with lower energy is more intense with an intensity ratio around 3:2. There is no apparent gap between the PW and ZPLs but the PW is much narrower than that of 0_0^0 transition. There are three other vibronic transitions, shifted by 19, 32, and 42 cm^{-1} from the strongest feature. These all have different peak shapes although they have comparable intensities.

A blow-up of the broad peak region around 27 000 cm^{-1} is presented in Figure 10. In addition to the previously mentioned eight a_1 normal modes, the modes and combination transitions
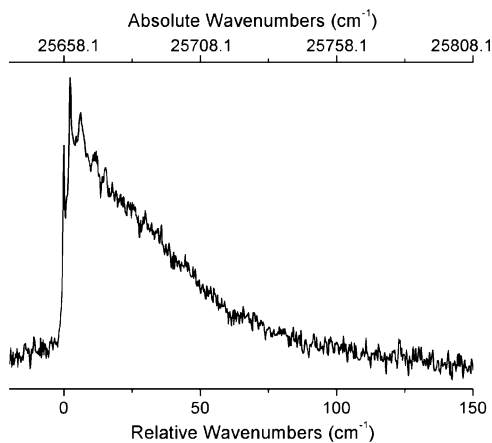
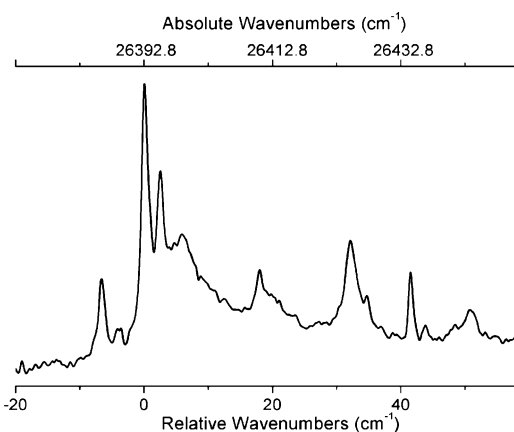**Figure 8.** The peak shape for the 0_0^0 transition of benzo(k)fluoranthene inside helium nanodroplets.

Figure 9. Expanded view of a typical vibronic band below 27 000 cm^{-1} for S$_1$ ← S$_0$ transition of benzo(k)fluoranthene in helium nanodroplets.
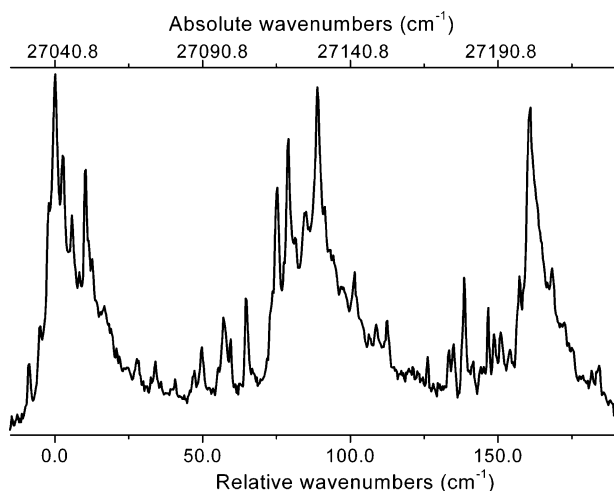

Figure 10. Expanded view of the broad structure around 27 000 cm^{-1} for S$_1$ ← S$_0$ transition of benzo(k)fluoranthene in helium nanodroplets.

yielding total symmetry of a_1, b_1, and b_2 are also allowed. It is unfortunate that the spectrum cannot be compared to the jet-cooled spectrum of the molecule for detailed comparison.

3.3.2. Benzo(k)fluoranthene van der Waals Complexes with Argon and Oxygen. The spectrum of the benzo(k)fluoranthene–oxygen van der Waals complex formed inside the helium droplets is shown in the vicinity of pure electronic transition in Figure 11. The 1:1 complex is observed as a relatively sharp line at about 40.2 cm^{-1} red-shifted from the monomer line. The
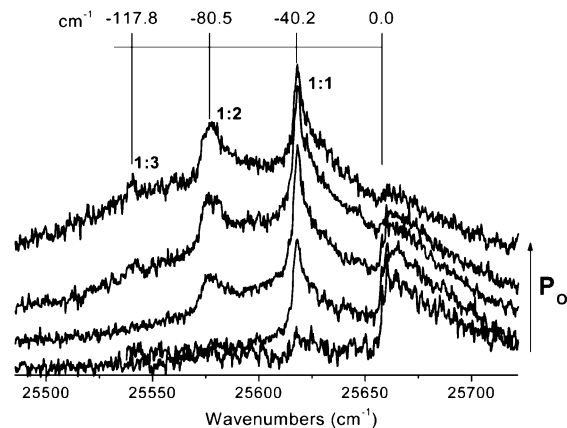

Figure 11. S$_1$ ← S$_0$ spectra of the benzo(k)fluoranthene–oxygen complex inside helium nanodroplets near the electronic origin.
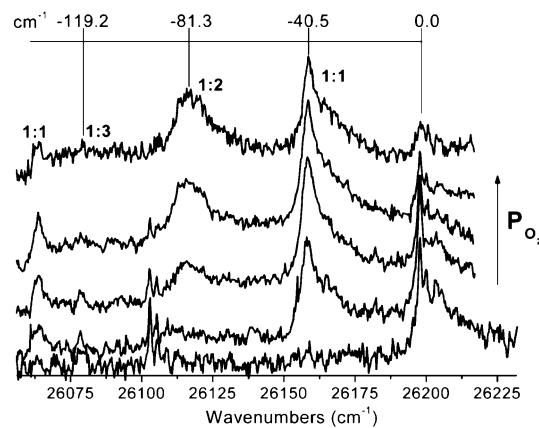

Figure 12. S$_1$ ← S$_0$ spectra of the benzo(k)fluoranthene–oxygen complex inside helium nanodroplets near ν_{19}.

complex peak does not show ZPL splitting. The peak is asymmetric with a PW extending about 25 cm^{-1}. Further increase of the pick-up pressure yields 1:2 complexes, which are rather broad with a fwhm = 12 cm^{-1} and are red-shifted by about 80.5 cm^{-1}. The amount of shift is about twice the 1:1 complex, and this situation agrees well with the additive property of polarizability shifts as demonstrated on perylene–rare gas complexes.[46] The larger width of the 2:1 complex probably arises from different structural isomers, including the cases when both oxygen molecules are on the same surface of benzo(k)-fluoranthene and on different surfaces. In the case of the perylene–argon complex, energies of such isomers differ only by 8 cm^{-1}, and it is not possible to resolve such isomers in this case inside helium droplets. The weak peak shifted about 117.8 cm^{-1} to the red can be assigned to a 1:3 complex because it is shifted almost by three times that of the 1:1 complex. The energy differences between structural isomers of the 1:3 complex should be larger; however, it not observed because of low signal intensity. For the 1:3 perylene–argon complex, the isomers of (1−2) and (0−3) argon distribution are separated by 22 cm^{-1}.

The benzo(k)fluoranthene–oxygen van der Waals complex spectrum near the 19_0^1 peak is shown in Figure 12. Although the 19_0^1 peak has a different shape than the 0_0^0 electronic transition, the oxygen complex has very similar shape. The 1:1 complex is observed at about 40.5 cm^{-1} with a width comparable to the main peak. There is no ZPL splitting, and the peak is more symmetric as compared to the complex observed near the electronic origin. The 1:2 complex shows up at −81.3 cm^{-1} to the red, and a weak 1:3 complex is observed at 119.2 cm^{-1}.

Nonalternant Hydrocarbons Inside Helium Nanodroplets

J. Phys. Chem. A, Vol. 111, No. 49, 2007 **12207**

TABLE 10: Equilibrium Positions and Energy Minima for Fluoranthene−Rare Gas Interactions
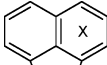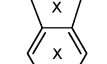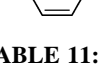
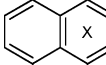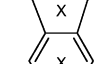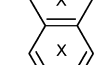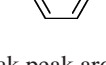| position	He	Ar
	3.21 Å −81.4 cm^{-1}	3.59 Å −364 cm^{-1}
	3.40 Å −70.1 cm^{-1}	3.75 Å −326 cm^{-1}
	3.20 Å −83.4 cm^{-1}	3.59 Å −369 cm^{-1}

TABLE 11: Equilibrium Positions and Energy Minima for Benzo(k)fluoranthene−Helium Interaction

position	He
	3.21 Å −81.4 cm^{-1}
	3.39 Å −70.2 cm^{-1}
	3.21 Å −80.1 cm^{-1}
	3.19 Å −85.4 cm^{-1}

The weak peak around 26 069 cm^{-1} is the 1:1 oxygen complex peak for the vibronic transition at 26 103 cm^{-1}.

The argon complex of benzo(k)fluoranthene, on the other hand, surprisingly did not yield any sharp structures.

4. Discussions

To explain the peak shapes of these molecules and their van der Waals complexes, it is desirable to have potential energy surfaces describing the interactions. Because we know of no ab inito potential for the molecules under consideration, we chose to approximate the interaction by extending results of benzene−rare gas pairs. We have used the angle dependent Lennard−Jones potential (6−12 for H−He; 8−14-θ for C−He), which was used by the Whaley group[13] to fit Hobza et al.'s second-order Møller−Plesset perturbation theory (MP2) level benzene−helium potential calculation.[47] The original potential predicts a global minima of −66.0 cm^{-1} above the center of the benzene ring at an equilibrium distance of 3.27 Å. We have scaled the parameters of this potential to match the most recent coupled-cluster with single and double and perturbative triple excitations (CCSD(T)) calculation, which places the global minima of D_e = −89.6 cm^{-1} at 3.16 Å above the center of the ring.[48] The form of the analytical fit is given in eqs 1−3. The new parameters are ϵ_{C-He} = 14.54 cm^{-1}, ϵ_{H-He} = 18.25 cm^{-1}, σ_{C-He} = 3.51 Å, and σ_{H-He} = 2.63 Å. The same analytical form was also used to calculate the interactions of the molecules with a single argon atom. The parameters, which were scaled to

match the latest CCSD(T) ground state benzene−argon interaction calculation,[49] are ϵ_{C-Ar} = 60.59 cm^{-1}, ϵ_{H-Ar} = 76.05 cm^{-1}, σ_{C-Ar} = 3.81 Å, and σ_{H-Ar} = 2.86 Å.

$$E_{C-He}(\vec{r}) = 4\epsilon_{C-He} \cos^2\theta\left[\left(\frac{\sigma_{C-He}\cos\theta}{|\vec{r}|}\right)^{14} - \left(\frac{\sigma_{C-He}\cos\theta}{|\vec{r}|}\right)^8\right] \quad (1)$$

$$E_{H-He}(\vec{r}) = 4\epsilon_{H-He}\left[\left(\frac{\sigma_{H-He}}{|\vec{r}|}\right)^{12} - \left(\frac{\sigma_{H-He}}{|\vec{r}|}\right)^6\right] \quad (2)$$

$$E_{benzene-He}(\vec{r}) = \sum_i E_{C-He}(\vec{r} - \vec{r}_i) + \sum_j E_{H-He}(\vec{r} - \vec{r}_j) \quad (3)$$

where θ is defined as the angle between the vector $(\vec{r} - \vec{r}_n)$ and the vector perpendicular to the molecular surface. A detailed comparison of the results this fit and the CCSD(T) calculations was reported previously.[16] We have not performed any calculations for the oxygen-containing complexes because the model Lennard−Jones potential for benzene−oxygen pairs[50] is not suitable for extension to larger systems.

These atomic−helium interactions were used to predict fluoranthene−helium and fluoranthene−Ar interaction potentials (see Table 10). For the fluoranthene−helium interaction, the absolute minima are over the benzene moiety and the secondary minima is over either ring of the naphthalene moiety. The interaction over the five-member ring is around 10% less attractive as compared to six-member rings. These differences arise from the stronger He−H than He−C attractions in the model. As has been discussed by Hartmann et al.,[6] the minima above adjacent benzene rings (∼2.5 Å, considerably less than the He−He equilibrium distance of 2.96 Å[12]) are too close to allow helium atoms to simultaneously occupy them without strong repulsive interactions. Thus, we expect that the ground state will have, on each side of the molecule, a helium atom localized over the benzene moiety and only one of the rings of the naphthalene moiety. This would give rise to two different possible isomers (depending upon whether the helium atoms on the naphthalene moiety are above the same or different rings), yet splitting of the ZPL is not observed. Localization of a helium atom over the five-member ring would displace helium atoms from above the six-member rings, and thus is expected to be a high-energy configuration of the liquid. Furthermore, argon and oxygen can localize over three different sites, over each type of ring.

Application of the same model calculations to the benzo(k)-fluoranthene-helium system predicts that the global minima are
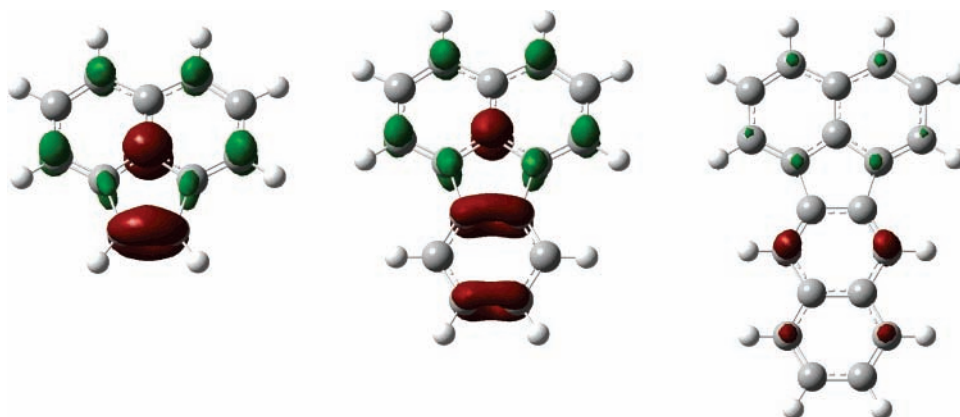
Figure 13. Electron density difference maps at 0.005 e/bohr^3.

over the last ring on the C_{2v} axis (see Table 11). The other three six-member rings are almost equivalent. As expected, the interaction with the five-member ring is not as attractive as the other rings. Possible permutations of helium atom localizations give rise to six different scenarios. These permutations can be grouped into three energetically close groups using the six-member rings on the C_{2v} axis. Most of the peaks have two apparent ZPLs (i.e., 0_0^0), and the reason why the peak shapes change with excess vibrational energy is not clear.

Electron density difference maps for $S_1 \leftarrow S_0$ transitions of the studied molecules are plotted in Figure 13 at the isosurface of 0.005 electrons/bohr³. Red and green signify decrease and increase in electron density, respectively. These maps are generated with GaussSum software,[51] which uses the output of a Gaussian TD−DFT calculation. Immediately noticeable is the different nature of the $S_1 \leftarrow S_0$ transition of benzo(k)-fluoranthene. Actually, as mentioned previously, the $S_2 \leftarrow S_0$ transition of benzo(k)fluoranthene correlates to the $S_1 \leftarrow S_0$ transition of the other two molecules. Although fluoranthene provides more possibilities for different solvation shell structures or localization scenarios due to its larger size, it has only one ZPL whereas acenaphtylene has split ZPLs. The recorded absolute signal for fluoranthene is higher but a strong PW is missing. Because both of these transitions are weak ($f = 0.006$ for acenaphtylene and 0.004 for fluoranthene, calculated at TD−DFT/B3LYP level) the observed transitions are far from saturation. The PW has been associated with the disturbance of the helium environment upon electronic excitation.[10] However, it is not clear why these molecules have different PW structures although they have similar electron density changes over the molecular plane. On the other hand, for benzo(k)-fluoranthene the PW is strong and wide. Because the allowed vibronic transitions for benzo(k)fluoranthene involve in-plane C−H bending modes, helium density around these bonds could be disturbed to yield strong PWs although the electron density over the molecular surface barely changes. However, this hypothesis does not explain why the 0_0^0 transition has a PW, even a broader one as compared to the rest of the vibronic bands.

5. Conclusions

The electronic spectra of acenaphtylene, fluoranthene, and benzo(k)fluoranthene have been recorded inside helium nanodroplets in the 24 500−27 500 cm⁻¹ spectral window using the beam depletion method. The $S_1 \leftarrow S_0$ transitions of these molecules inside helium droplets exhibit different lineshapes.

Acenaphtylene has multiple ZPLs riding on a broad background. A qualitatively similar (thought more compact) line shape was previously observed for the $S_1 \leftarrow S_0$ transition of perylene inside helium droplets with a narrow line width laser excitation. Considering the large size difference between these two molecules, this similarity is puzzling and stimulating.

The fluoranthene transitions show a single sharp ZPL, followed by a weak peak and a PW. The position of the PW is comparable to previous observations. Although the line shape of the molecule itself does not have any peculiar aspects, the oxygen and argon van der Waals complexes have surprisingly more peaks than the number of possible unique binding positions.

Benzo(k)fluoranthene has different lineshapes for the purely electronic transition and the rest of the vibronic bands. The 0_0^0 transition has partially split ZPLs with a broad PW. The vibronic transitions, on the other hand, have better resolved ZPLs and a weaker PW. Furthermore, the intensity ratio for the ZPLs is opposite for these two cases. The lineshapes of the oxygen van

der Waals complex for the 0_0^0 and the vibronic transitions, however, are similar with almost the same amount of spectral shifts.

The presented spectra of these three molecules and their van der Waals complexes are unique cases despite the similarities among them. The observations cannot be accounted for with the current level of understanding of the helium solvation. Obviously, more work, both experimental and theoretical, needs to be done before one can predict the outcome of such experiments.

Supporting Information Available: Table of relative intensities. This material is available free of charge via the Internet at http://pubs.acs.org.

Note Added after ASAP Publication. This Article was published on Articles ASAP on September 20, 2007. A Supporting Information paragraph was added, and the paper was reposted with the issue on December 6, 2007.

References and Notes

(1) Schmied, R.; Carcabal, P.; Dokter, A. M.; Lonij, V. P. A.; Lehmann, K. K.; Scoles, G. *J. Chem. Phys.* **2004**, *121*, 2701.

(2) Boatwright, A.; Besley, N. A.; Curtis, S.; Wright, R. R.; Stace, A. J. *J. Chem. Phys.* **2005**, *123*, 21102.

(3) Lindinger, A., Vibronische Spektroskopie von Organischen und Biologischen Molekulen in 4Helium-Clustern Ph.D. Thesis, Georg-August-Universitaet, 1999.

(4) Krasnokutski, S.; Rouille, G.; Huisken, F. *Chem. Phys. Lett.* **2005**, *406*, 386.

(5) Hartmann, M.; Lindinger, A.; Toennies, J. P.; Vilesov, A. F. *Chem. Phys.* **1998**, *239*, 139.

(6) (a) Hartmann, M.; Lindinger, A.; Toennies, J. P.; Vilesov, A. F. *J. Phys. Chem. A* **2001**, *105*, 6369. (b) Lehnig, R.; Slenczka, A. *J. Chem. Phys.* **2003**, *118*, 8256; **2004**, *120*, 5064.

(7) Lindinger, A.; Toennies, J. P.; Vilesov, A. F. *Phys. Chem. Chem. Phys* **2001**, *3*, 2581.

(8) Hartmann, M.; Lindinger, A.; Toennies, J. P.; Vilesov, A. F. *Phys. Chem. Chem. Phys* **2002**, *4*, 4839.

(9) Lehnig, R.; Slenczka, A. *J. Chem. Phys.* **2005**, *122*, 244317.

(10) Hartmann, M.; Mielke, F.; Toennies, J. P.; Vilesov, A. F.; Benedek, G. *Phys. Rev. Lett.* **1996**, *76*, 4560.

(11) Svensson, E. C.; Sears, V. F.; Woods, A. B. D.; Mortel, P. *Phys. Rev. B* **1980**, *21*, 3638.

(12) Janzen, A. R.; Aziz, R. a. *J. Chem. Phys.* **1997**, *107*, 914.

(13) Kwon, Y.; Whaley, K. B. *J. Chem. Phys.* **2001**, *114*, 3163.

(14) Huang, P.; Whitley, H. D.; Whaley, K. B. *J. Low Temp. Phys.* **2004**, *134*, 263.

(15) Whitley, H. D.; Huang, P.; Kwon, Y.; Whaley, K. B. *J. Chem. Phys.* **2005**, *123*, 054307.

(16) Birer, O.; Moreschini, P.; Lehmann, K. K.; Scoles, G. *J. Phys. Chem. A* **2007**, *111*, 7624−7630.

(17) Heilbronner, E.; Weber, J. P.; Michl, J.; Zahradni, R. *Theo. Chim. Acta* **1966**, *6*, 141.

(18) Nakhimovsky, L. A.; Iamotte, M.; Joussot-Dubien, J. *Handbook of Low Temperature Electronic Spectra of Polycyclic Aromatic Hydrocarbons*; Elsevier: New York, 1989.

(19) Chan, I. Y.; Dantus, M. *J. Chem. Phys.* **1985**, *82*, 4771.

(20) Callegari, C.; Lehmann, K. K.; Schmied, R.; Scoles, G. *J. Chem. Phys.* **2001**, *115*, 10090.

(21) Knuth, E. L.; Schilling, B.; Toennies, J. P., In *19th International Symposium on Rarefied Gas Dynamics*; Harvey, J., Lord, G., Eds; Oxford University Press Inc: Oxford, 1995; Vol. 19, p 270.

(22) Infrared Laboratories, Tucson, AZ.

(23) Positive Light, Inc., Los Gatos, CA.

(24) Littman, M. G. *Opt. Lett.* **1978**, *3*, 138.

(25) EXFO Burleigh Products Group, Inc., Victor, NY.

(26) National Instruments Corp., Austin, TX.

(27) Foresman, J. B.; Head-Gordon, M.; Pople, J. A.; Frisch, M. *J. Phys. Chem.* **1992**, *96*, 135.

(28) *Gaussian 03*, Rev C.02, Frisch, M. J.; Trucks, G. W.; Schlegel, H. B.; Scuseria, G. E.; Robb, M. A.; Cheeseman, J. R.; Montgomery, J. J. A.; Vreven, T.; Kudin, K. N.; Burant, J. C.; Millam, J. M.; Iyengar, S. S.; Tomasi, J.; Barone, V.; Mennucci, B.; Cossi, M.; Scalmani, G.; Rega, N.;

Nonalternant Hydrocarbons Inside Helium Nanodroplets

J. Phys. Chem. A, Vol. 111, No. 49, 2007 **12209**

Petersson, G. A.; Nakatsuji, H.; Hada, M.; Ehara, M.; Toyota, K.; Fukuda, R.; Hasegawa, J.; Ishida, M.; Nakajima, T.; Honda, Y.; Kitao, O.; Nakai, H.; Klene, M.; Li, X.; Knox, J. E.; Hratchian, H. P.; Cross, J. B.; Bakken, V.; Adamo, C.; Jaramillo, J.; Gomperts, R.; Stratmann, R. E.; Yazyev, O.; Austin, A. J.; Cammi, R.; Pomelli, C.; Ochterski, J. W.; Ayala, P. Y.; Morokuma, K.; Voth, G. A.; Salvador, P.; Dannenberg, J. J.; Zakrzewski, V. G.; Dapprich, S.; Daniels, A. D.; Strain, M. C.; Farkas, O.; Malick, D. K.; Rabuck, A. D.; Raghavachari, K.; Foresman, J. B.; Ortiz, J. V.; Cui,Q.; Baboul, A. G.; Clifford, S.; Cioslowski, J.; Stefanov, B. B.; Liu, G.; Liashenko, A.; Piskorz, P.; Komaromi, I.; Martin, R. L.; Fox, D. J.; Keith, T.; Al-Laham, M. A.; Peng, C. Y.; Nanayakkara, A.; Challacombe, M.; Gill, P. M. W.; Johnson, B.; Chen, W.; Wong, M. W.; Gonzalez, C.; Pople, J. A.; Gaussian, Inc.: Wallingford, Connecticut, 2004.

(29) Thulstrup, E. W.; Michl, J. *J. Am. Chem. Soc.* **1976**, *98*, 4533.

(30) Kenney, J. W.; Herold, D. a.; Michl, J.; Michl, J. *J. Am. Chem. Soc.* **1978**, *100*, 6884.

(31) Banisaukas, J.; Szczepanski, J.; Eyler, J.; Vala, M.; Hirata, S.; Head-Gordon, M.; Oomens, J.; Meijer, G.; von Helden, G. *J. Phys. Chem. A* **2003**, *107*, 782.

(32) Radziszewski, J. G.; Abildgaard, J.; Thulstrup, E. W. *Spectrochim. Acta A* **1997**, *53*, 2095.

(33) Wood, R. a.; Welberry, T. R.; Rae, A. D. *J. Chem. Soc. Perkin Trans. 2* **1985**, 451.

(34) Maddams, W. F.; Schnurmann, R. *J. Chem. Phys.* **1951**, *19*, 973.

(35) Philen, D. L.; Hedges, R. M. *Chem. Phys. Lett.* **1976**, *43*, 358.

(36) Kolc, J.; Thulstru.Ew; Michl, J. *J. Am. Chem. Soc.* **1974**, *96*, 7188.

(37) Hudgins, D. M.; Sandford, S. A. *J. Phys. Chem. A* **1998**, *102*, 353.

(38) Klaeboe, P.; Cyvin, S. J.; Asbjornsen, A. P.; Cyvin, B. N. *Spectrochim. Acta A* **1981**, *37*, 655.

(39) Havenith, R. W. A.; van Lenthe, J. H.; Jenneskens, L. W. *J. Org. Chem.* **2005**, *70*, 4484.

(40) Pesteil, L.; Pesteil, P.; Laurent, F. *Can. J. Chem.* **1964**, *42*, 2601.

(41) Hazell, a. C.; Jones, D. W.; Sowden, J. M. *Acta Crystallogr., Sect. B* **1977**, *33*, 1516.

(42) Higgins, J. P., Helium Cluster Isolation Spectroscopy. Ph.D. Thesis, Princeton University, 1998.

(43) Michl, J.; Eggers, J. H. *Tetrahedron* **1974**, *30*, 813.

(44) Souto, M. a.; Otteson, D.; Michl, J. *J. Am. Chem. Soc.* **1978**, *100*, 6892.

(45) Cobb, W. T.; Mcgown, L. B. *Anal. Chem.* **1990**, *62*, 186.

(46) Bahatt, D.; Heidenreich, a.; Benhorin, N.; Even, U.; Jortner, J. *J. Chem. Phys.* **1994**, *100*, 6290.

(47) Hobza, P.; Bludsky, O.; Selzle, H. L.; Schlag, E. W. *J. Chem. Phys.* **1992**, *97*, 335.

(48) Lee, S.; Chung, J. S.; Felker, P. M.; Cacheiro, J. L.; Fernandez, B.; Pedersen, T. B.; Koch, H. *J. Chem. Phys.* **2003**, *119*, 12956.

(49) Koch, H.; Fernandez, B.; Makarewicz, J. *J. Chem. Phys.* **1999**, *111*, 198.

(50) Granucci, G.; Persico, M. *Chem. Phys. Lett.* **1993**, *205*, 331.

(51) O'Boyle, N. M.; Vos, J. G. *GaussSum1.0*; http://gaussum.source-forge.net, Dublin City University, 2005.